ISSN 0915-633X

NATIONAL INSTITUTE FOR FUSION SCIENCE

Spectral Analysis of the Heliotron Field with the Toroidal Harmonic Function in a Study of the Structure of Built-in Divertor

H. Kaneko

(Received – Dec. 12, 1990)

NIFS-71 Jan. 1991

RESEARCH REPORT
NIFS Series

NAGOYA, JAPAN

Spectral Analysis of the Heliotron Field with the Toroidal Harmonic Function in a Study of the Structure of Built-in Divertor

H. Kaneko

National Institute for Fusion Science,
Furo-Cho, Chikusa-Ku, Nagoya 464-01, Japan

Abstract

Representation of the vacuum magnetic field by a set of harmonic functions is useful for an analysis of a magnetic configuration. To analyse a helical configuration precisely, a harmonic function describing a pure helicity of the configuration is desired specially in heliotrons, where the good quasi-symmetry is regarded as an advantage for a helical built-in divertor. Owing to the specific mode numbers in both the toroidal and the poloidal directions, the toroidal harmonic function is appropriate for a study of the helical field, when a practical method for a numerical calculation is provided. The helical components are analysed by a numerical calculation with high accuracy. From a spectral analysis of the field generated by a continuous helical coil the natural winding law was found to be peculiar by the fact that only the components resonant with the helicity of the coil are dominant. A deviation from the natural winding law, such as in a traditional winding law, causes an enhancement of off-resonant components. The unique toroidal coordinates, and hence, the unique spectral representation is practically determined from the condition that the field expression by a spectral series has the maximum area for the convergence. The high accuracy of the representation was applied to a numerical investigation of the intricate structure of a helical divertor. A reticular structure of the scrape-off layer in a helical system is visualized with a trace of unclosed separatrix. The field line at the X-point is a nearly pure helix in the toroidal coordinates, and it was confirmed that the deviation is sufficiently small for divertor baffles to be rigidly installed, even when some additional field is expected in an experiment.

I. Introduction

It is well known that a magnetic field in a vacuum has a scalar potential $\Phi(x,y,z)$. It is frequently useful for a study of magnetic confinement to analyse the potential satisfying the Laplace equation by a series of harmonic functions characterizing the magnetic components involved. The analysis is, unfortunately, not always convenient for axi-asymmetric torus. Since the magnetic configuration is rather primitively determined by a coil configuration, the coil configuration has been directly studied for a design of an axi-asymmetric device[1-6]. Various but particular coil configurations have been studied for a design of Large Helical Device(LHD)[3], or the next generation heliotron in Japan, so far. Since such studies are concerned with only an typical coil shape, systematic survey on various coil system is apt to remain insufficient compared with its large number of adjustable parameters in the configuration. So, it is still worth trying to describe the result from the analyses with respect to a common characteristic or a universal definition of the magnetic configuration.

Even in a three-dimensional magnetic configuration, some symmetry is still retained in a practical device. Then, it is used as a basis of the analysis. Besides the use of the toroidal coordinates, which is a natural choice for a toroidal configuration, the assumption that a configuration has rotational symmetry of order M defines the unique z-axis. Thus, we start from a series of harmonic components[7-10] by

$$\Phi(u,v,w)=\sum_{j,n=-\infty}^{\infty} a_{j,n}\sqrt{D}\,Q^{|j|M}_{|n|-1/2}(\cosh v)\exp i(jMw+nu)+bw. \tag{1}$$

Here, (u,v,w) are the toroidal coordinates: $x=(c/D)\sinh v\cos w$, $y=(c/D)\sinh v\sin w$, $z=(c/D)\sin u$ and $D=\cosh v-\cos u$. Q's are the torus functions. The relation $a_{-j,-n}=a_{j,n}^{*}$ is assumed to keep the potential real. And, bw corresponds to the toroidal field causing the multi-valued feature of the potential. Then, a set of relative components $a_{j,n}/b$ characterizes the magnetic configuration. However, a change in the constant c yields a different set of components. Since one of the aims is to label each configuration, it is intrinsic to fix c. The conclusive method has not been found, and the practical choice of c will be shown later.

The advantage of the definition by harmonic components in a configuration study is emphasized in the optimization of modular stellarators[11,12]. However, use of the torus function was avoided there because of, presumably, a numerical calculation of the unfamiliar function. Although there might be a great difference in the calculation time, the advantage will be common. Hence, what has been desired is a practical method for the calculation. The torus functions and their numerical calculation employed here are summarized in Appendix.

The peculiar advantage in the expression by the toroidal harmonic functions is that each component is a global mode with intrinsic mode numbers. The expression is, hence, a spectral analysis of the field. In a device with a continuous helical coil such as in heliotrons there is a helical mode dominant in the concerning area. The field is most conveniently expressed by eigen modes in the toroidal coordinates where both toroidal and poloidal mode numbers are separated. Also, the clear global mode numbers of the eigen mode are essential in a study of a helical built-in divertor, because it requires a clear helical field near the plasma boundary as well as in the confinement region. Thus, the use of toroidal harmonic functions has a great advantage as a common base for both a study of magnetic confinement and that of helical divertor. The spectral expression will be a better choice for a systematic study of heliotrons.

When a continuous helical coil is used, the dominant component is determined by the repetition number of the coil. When the number is kept unchanged, the major possibility in an optimization study is a small modification of the mixture of the components. Sensitivity check by an arbitrary change in a particular component is effective to survey a preferable modification in the coil configuration. Then, the correct analysis of the exact field generated by the coil system and the understanding of a spectral change due to the coil modification is essential for a subsequent optimization study.

Beside the use for a definition of a configuration and for an arbitrarily adjustable model, the high accuracy as a model is peculiarly applicable to an investigation of an X-point. The understanding of an X-point is very important for a design of a divertor. However, lack of symmetry, and hence, lack of magnetic surface, in a helical system causes a very intricate structure near the X-point. Moreover, since the field has a strong shear near the X-point, quite high accuracy is required for a numerical study of the structure. The present calculation is not yet enough for the purpose. However, the structure was investigated with sufficiently high accuracy by the field trace together with a linearized approximation of the field mapping.

The use of the toroidal harmonic function is briefly reviewed in Sec.II.

The spectral analysis of a heliotron field is demonstrated in Sec.III. Spectral change due to coil modification is investigated in Sec.IV. An X-point and the structure of a helical divertor in the model field are investigated in Sec.V. Summary and related discussion are given in Sec.VI.

II. Spectral representation of toroidal magnetic configuration

The magnetic field is given by the derivative with respect to the cartesian coordinates (x,y,z), and, more importantly, magnetic surfaces are given by solving differential equations:

$$\frac{dx}{\partial\Phi/\partial x}=\frac{dy}{\partial\Phi/\partial y}=\frac{dz}{\partial\Phi/\partial z} \qquad (2)$$

with a not-well-posed boundary condition. Since the toroidal coordinates are orthogonal, the equation can be easily translated to the expression with $(u_j)=(u,v,w)$ as that $\frac{g_j^2 du_j}{\partial\Phi/\partial u_j}$ are equal among j=1,2 and 3, where $g_j^2=g_{jj}$ is the first fundamental quantity.

$$\frac{\partial\Phi}{\partial u}=\sum_{j,n=-\infty}^{\infty} a_{j,n}\left(\frac{\sin u}{2D}+in\right)\sqrt{D}Q^{|j|M}_{|n|-1/2}(\cosh v)\exp i(jMw+nu) \qquad (3)$$

$$\frac{\partial\Phi}{\partial v}=\sum_{j,n=-\infty}^{\infty} a_{j,n}\{[\frac{\sinh v}{2D}-(|n|+\frac{1}{2})\coth v]\sqrt{D}\ Q^{|j|M}_{|n|-1/2}(\cosh v)$$
$$+(|n|-|j|M+\frac{1}{2})\,\mathrm{cosech}\, v\sqrt{D}\ Q^{|j|M}_{|n|+1/2}(\cosh v)\}\exp i(jMw+nu) \qquad (4)$$

$$\frac{\partial\Phi}{\partial w}=\sum_{j,n=-\infty}^{\infty} ijMa_{j,n}\sqrt{D}Q^{|j|M}_{|n|-1/2}(\cosh v)\exp i(jMw+nu)+b \qquad (5)$$

Thus, a field line is easily traced numerically also in the toroidal coordinates. However, the coordinate v is not convenient, because the magnetic surface contains the point $v=\infty$. In stead of v, new variable $\rho=c/\sinh v$, or the minor radius of the torus, was used. The constant factor in a harmonic function is of no interest, and another function:

$$\mathcal{Q}^j_n(\rho;M,c)=\frac{\rho^{|n|}}{(c^2+\rho^2)^{|n|/2}}q_{|j|M,|n|}\left(\frac{(c^2+\rho^2)^{1/2}}{\rho}\right) \qquad (6)$$

was employed (See Appendix for the definition of $q_{m,n}$). This function will be sometimes referred in this article with some or all parameters unspelled for simplicity, unless any confusion occurs. Now, using re-adjusted coefficient

$a_{j,n}$, which is different in numerical value from that in Eq.(1), the magnetic potential is concisely expressed by

$$\Phi(\rho,u,w)=\sum_{j=0}^{\infty}\sum_{n=-\infty}^{\infty}\Delta^{1/2}[a_{j,n}\sin(jMw+nu)+a'_{j,n}\cos(jMw+nu)]\mathcal{Q}+bw, \tag{7}$$

where $\Delta=1-\frac{\rho}{(c^2+\rho^2)^{1/2}}\cos u$.

The terms with a cosine function do not appear in this article and are omitted in the following equations. Now, Eq.(2) becomes

$$\frac{c^2}{\Delta(c^2+\rho^2)}\frac{d\rho}{B_\rho}=\frac{c\rho}{\Delta(c^2+\rho^2)^{1/2}}\frac{du}{B_u}=\frac{c^2}{\Delta(c^2+\rho^2)^{1/2}}\frac{dw}{B_w}, \tag{8}$$

where B_ρ, B_u and B_w are each component of the magnetic field:

$$B_\rho=\frac{\Delta(c^2+\rho^2)^{1/2}}{c\rho}\sum_{j=0}^{\infty}\sum_{n=-\infty}^{\infty}\Delta^{1/2}a_{j,n}\{[\frac{1}{2\Delta}\frac{c}{(c^2+\rho^2)^{1/2}}-(|n|+\frac{1}{2})\frac{(c^2+\rho^2)^{1/2}}{c}]\mathcal{Q}_n$$
$$+(|n|-jM+\frac{1}{2})\frac{\rho}{c}\frac{|n|+jM+1/2}{2|n|+1}\mathcal{Q}_{n+1}\}\sin(jMw+nu) \tag{9}$$

$$B_u=-\frac{\Delta(c^2+\rho^2)^{1/2}}{c\rho}\sum_{j=0}^{\infty}\sum_{n=-\infty}^{\infty}\Delta^{1/2}a_{j,n}[\frac{\sin u}{2\Delta}\frac{\rho}{(c^2+\rho^2)^{1/2}}\sin(jMw+nu)+n\cos(jMw+nu)]\mathcal{Q} \tag{10}$$

$$B_w=-\frac{\Delta(c^2+\rho^2)^{1/2}}{c^2}[\sum_{j=0}^{\infty}\sum_{n=-\infty}^{\infty}jM\Delta^{1/2}a_{j,n}\mathcal{Q}\cos(jMw+nu)+b] \tag{11}$$

Thus, it is generally possible to define a toroidal configuration by the scale factor c, the strength factor b and a set of the spectral components $a_{j,n}$ except in a helical-axis configuration. If the helical magnetic axis is out of the range of convergence of the series, it is inconvenient to use the series for a definition of the magnetic configuration. The situation is the same in an arbitrary toroidal configuration without any symmetry, because it is a particular case with $M=1$. Of course, the validity is restricted by the convergence in any case.

III. Spectral analysis of heliotron field

Magnetic fields generated by a particular coil system is usually calculated by a numerical integration of the Biot-Savart's formula. If the magnetic field is given, it is easy to analyse the field, because B_w in Eq.(11) is the toroidal field and the analysis corresponds exactly to a fourier transform. Since it is not a present interest to investigate a particular coil system, a filament current is considered first. The trajectory is on a torus with the major radius

R_c and the minor radius a_c and is defined by a winding law $\varphi=(l/M)K(\theta)$, as shown in Fig.1, where l is the poloidal repetition number of the filament, φ is the toroidal angle and θ is the poloidal angle. To obtain high accuracy, an especial method was used. The current was expressed as a sum of basic current loops. Excess currents on rings were easily subtracted. The magnetic potential due to the loop Δ in Fig.1 is expressed as

$$\Phi(\rho,u,w)=\int\int_\Delta \frac{d\varphi d\theta}{R^3}\begin{bmatrix} -(R_c+a_c\cos\theta)\sin\varphi \\ (R_c+a_c\cos\theta)\cos\varphi \\ 0 \end{bmatrix}\times\begin{bmatrix} -a_c\sin\theta\cos\varphi \\ -a_c\sin\theta\sin\varphi \\ a_c\cos\theta \end{bmatrix} \cdot\begin{bmatrix} r\cos w-(R_c+a_c\cos\theta)\cos\varphi \\ r\sin w-(R_c+a_c\cos\theta)\sin\varphi \\ z-a_c\sin\theta \end{bmatrix}$$

$$=\int\int_\Delta F(\theta,\varphi;\rho,u,w)d\theta d\varphi, \tag{12}$$

where $R=\sqrt{(R_c+a_c\cos\theta)^2+r^2-2r(R_c+a_c\cos\theta)\cos(\varphi-w)+(a_c\sin\theta-z)^2}$, and

$$F(\theta,\varphi;\rho,u,w)=a_c(R_c+a_c\cos\theta)\frac{z\sin\theta+r\cos\theta\cos(\varphi-w)-(R_c\cos\theta+a_c)}{R^3}.$$

Here r and z are regarded as a function of ρ and u, and the factor $\mu_0 I/4\pi$ is normalized to unity for simplicity.

A 2-dimensional integration is not convenient for a numerical calculation. Remembering that the toroidal field is useful for the analysis, the components with $j\neq 0$ were calculated from

$$\frac{\partial\Phi}{\partial w}=\int\int_\Delta\frac{\partial F}{\partial w}d\theta d\varphi$$

$$=-\int\int_\Delta\frac{\partial F}{\partial\varphi}d\theta d\varphi$$

$$=\int_0^\pi d\theta[F(\theta,0;\rho,u,w)-F(\theta,\frac{l}{M}K(\theta);\rho,u,w)]. \tag{13}$$

Remaining components with $j=0$ (poloidal field) were calculated from an azimuthally averaged potential. The central axis in the coordinates is defined here by $c=\sqrt{R_c^2-a_c^2}$. As known well, a harmonic function is uniquely determined from the values on an appropriate surface and can be analytically extended to the neighborhood. So, the magnetic field or the potential on only a torus with $\rho=0.8a_c$ was used for this spectral analysis. The distribution of the spectral components on the surface at the coil radius normalized by toroidal field b, or $a_{j,n}Q(\rho=a_c)/b$, is displayed in Fig.2, where only the absolute value is plotted in a logarithmic scale. The case of M=10 and l=2 is implicitly assumed in this article. Figure 2a shows the spectral distribution for the simple winding with right-handed screw: $K(\theta)=-\theta$. The random base shows the error level. Five ridges can be recognized. A pair of ridges are located along each constant-n/j line with $n>0$. Two with $n<0$ are fault images of extension of the above two ridges due to the fourier transform truncated at a finite mode number. And, the other small one at $n=0$ is presumably the ghost of $n=64$ components by the same reason. Thus, only the former two ridges correspond to the actual spectral components. The magnetic field is composed of a wide range of spectral components even when a simple helical winding is used. Since the coil is symmetric (the current is anti-symmetric) with respect to the inversion against x-axis, the other asymmetric parts are not significant and are not displayed in the figure. The asymmetric components [terms with a cosine function in Eq.(7)] are not dealt with at all in this article.

As will be expected, a simple spectral distribution from a filament current is obtained when a simple winding law in the (u,w)-plane rather than in the (θ,φ)-plane is employed. Figure 2b shows the case with the *natural* winding: $w=-(M/l)u$ (c is defined such that the coil is on the constant-ρ surface at $\rho=a_c$). Now the main two ridges are combined into one, and the ridge becomes sharp. The ridge is exactly on the $n/j=2$ line. This means that only the field resonant with the coil helicity is dominant. Thus, it was found that a good quasi-symmetry is expected by the natural winding. The other component is smaller than the resonant component by an order of magnitude.

There is a difficulty in a calculation of the magnetic field from these components, even if the higher-n components are correctly processed. The peak values on the ridge in Fig.2b approach to a finite constant as j increases. This means that the series does not converge on the surface $\rho=a_c$. It is due to a singularity at the current filament. Thus, the convergence radius of the series is a_c and the series converges at any radius less than a_c. The field near the convergence radius must be calculated carefully, because the convergence of the series is very slow. Such a calculation was not tried here.

The magnetic configuration of a plasma is characterized by dominant components in the confinement region. Since the higher-mode component increases rapidly with the radius, and becomes, at most in the case of filament current, comparable in strength at the coil surface, the contribution to the plasma configuration is usually small. The practical application is made by truncating the series at an appropriate value in j and n. The difference between the magnetic field calculated by a finite series, with $j<16$ and $n<32$ in particular, and the other by Biot-Savart's formula is shown in Fig.3. The difference inside the coil surface is roughly proportional to $(\rho/a_c)^{32}$. The coefficient depends on the coil configuration, and becomes small when a realistic coil with a finite size is taken into account. Thus, the inclusion or exclusion of a particular component in a calculation must be carefully decided depending on the problem under consideration.

IV. Modulation in helical winding

Magnetic configuration of a helical device is mainly controlled by a choice of a winding law of the helical coil[4]. The spectral components in two particular configurations have been already shown. To discuss a possible modification of the spectral components, modulation of the winding law. particularly infinitesimal modulation, was investigated. The winding law is assumed to have a pitch modulation $\alpha f(\theta)$ with a small parameter α as

$$\varphi=\frac{l}{M}[K(\theta)+\alpha f(\theta)], \tag{15}$$

where the constraint $f(0)=f(\pi)=0$ is assumed. Of course, if the modulation is included into $K(\theta)$, nothing new occurs. The pattern of a spectral change is of interest now. The change $\Delta\Phi$ due to the unit current loop is given in the first order of α as

$$\Delta\Phi=\alpha\int F(\theta,\frac{l}{M}K(\theta);\rho,u,w)f(\theta)d\theta, \tag{16}$$

where the function F has been already used in Eq.(12). Figure 4a shows the spectral components for the natural winding again but in the linear scale. The $j=0$ components are excluded from the discussion, because they are independently controlable by poloidal-field coils. As already noted, the components with $n=2j$ are dominant. The sign of the coefficient is the same among all dominant terms. Since too-steep modulation is not accessible in an actual device, slowly varying modulation is important for a design. Two cases of a basic modulation with $f(\theta)=\sin u$ and $f(\theta)=\sin 2u$ are displayed in Figs.4b and 4c, respectively, where u is regarded as a function of θ by the relation of the natural winding. Owing to the purity of the spectral structure, it is clearly seen that the modulation of $\sin u$ affects the components with odd n mode number , while the other affects those with even n. More precisely, the components with $n=2j\pm1$ are affected by the former modulation and those with $n=2j\pm2$ are affected by the latter. A steep profile like a derivative of a δ-function as a function of n implies that the linear response from infinitesimal modulation must not be applied to finite modulation. If the origin of the δ-function moves with an increase of the modulation, subsequent modulation up to a finite amplitude might cause a positional shift of the distribution rather than a proportional change in amplitude. This can be speculated from Fig.2a.

Another basic modulation is the radial modulation of the winding. The radius a was defined as a function of θ by

$$a=a_c[1+\alpha g(\theta)], \tag{17}$$

where the similar constraint $g(0)=g(\pi)=0$ was employed. The change due to infinitesimal modulation is given by

$$\Delta\Phi=\alpha\int\frac{ra_c\sin(\varphi-w)+rc\sin\theta\cos(\varphi-w)-z\cos\theta-R_c c\sin\theta}{R^3}g(\theta)d\theta. \tag{18}$$

Here, the natural winding is already assumed. Two cases with $g(\theta)=\sin^2 u$ and $g(\theta)=\sin u\sin 2u$ were investigated. Obtained pattern was much more complicated than that in Fig.4. No understanding was obtained other than that the former modulation affects the odd n components whereas the latter affects the even n components. Since components in a wide range of the mode number are affected simultaneously, it is rather difficult to use this modulation for an intended control of the spectral composition.

There is another interest in the case that $g(\pi)$ is not zero. If c is re-adjusted, the case is included in the previous case. So, the problem is what is the spectral component in a frame with a different value of c. Figure 5 shows the result from a slightly larger $c=(R_c+\sqrt{R_c^2-a_c^2})/2$ for the case of the natural winding. Since the analysis is not valid beyond the location of the current, the convergence radius is now less than a_c. Hence, the spectral components evaluated at the equivalent radius diverge as the mode number increases. If a slightly too-small value of c is used, the change is similar. At any rate, the magnetic configuration defined by each of those spectral distributions is identical. The apparent difference among them is not intrinsic. Hence, it is necessary to fix c uniquely. Here, it was determined by the condition that the torus inscribed to the current carrying area coincides with a constant-ρ surface. Besides a theoretical interest where the components are arbitrarily selected, the configuration from a real coil system is thus uniquely determined. Since the series in this frame have the largest convergence radius than in any other one, it can be said that high-mode components have the minimum strength in the frame.

Starting from the simple winding, two parameters, or the pitch angle

$\gamma_c=(M/l)(a_c/R_c)$ and the pitch modulation α^*, have been carefully selected in the design study of LHD[3,13]. Now, the effect of a change in those parameters can be quantitatively discussed with the change in the spectral components. Since the broadening of the spectrum makes the difference unclear, the natural winding model was employed as a standard for the comparison. The first four components with $n/j=2$ and the $n=1/j=1$ component are plotted as a function of γ_c in Fig.6. The increase in γ_c decreases helical components relative to the toroidal field. Hence, the controlable γ_c in the LHD operation is the alternative to an additional toroidal coil system[14]. However, it should be noted that the simultaneous change in other components must be taken into account. Larger γ_c gives a simple configuration with smaller higher-mode components, but also a helical excursion of the magnetic axis due to the $n=1$ component becomes relatively significant in comparison under the limited condition of no poloidal fields.

The LHD winding is defined by the other parameter α^* as

$$\theta=\frac{M}{l}\varphi+\alpha^* \sin\left(\frac{M}{l}\varphi\right). \tag{14}$$

It is responsible for a control of wide range of higher-mode components. Some typical winding laws are plotted on the w-u plane in Fig.7. Of course, the natural winding is the simplest one in this frame. It was confirmed that a split into the two main ridges in Fig.2a with $n/j=1.56$ and 2.52 corresponds exactly to the broadening of the gradient; $M dw/du=lc/(R_c\pm a_c)$.

Magnetic configuration of LHD has been decided within the parameter space γ_c and α^*. It has not yet, however, been certain whether the survey on the configuration was sufficient or not. The *simple* winding is almost a modulation from the *natural* winding of the type $\sin u$. It includes the odd-n components comparable with the others. A nearly natural winding is attained by a selection of $\alpha^*=0.2$ or more in this case with $\gamma_c=1.25$. However, the compromise among the confinement of a high energy particle and the beta limit due to stability resulted in the choice of an intermediate value $\alpha^*=0.1$ for LHD[13]. The choice of moderate α^* means that the compensation of the odd-n components is not sufficient.

When a finite-sized coil is used, the configuration becomes far rich in variation. For example, if the coil shape is a ribbon on the torus and the width of the ribbon is defined by constant $\Delta\varphi$ at the intersection with every horizontal plane, any spectral component of $A_{j,n}$ is easily deduced from that for a filament model as

$$A_{j,n}=a_{j,n}\frac{2}{|j|M\Delta\varphi}\sin\frac{|j|M\Delta\varphi}{2}. \tag{20}$$

Thus, spectral components with a high j-number becomes less important, when the coil with a finite size is considered. The value of the sine function is interesting for its randomness. For large j, the sign and value depends on the small change in $\Delta\varphi$. Since a drastic change in plasma behaviour is not expected from such a minor change in the coil shape, a high-j component or, at least, the individual component will not be responsible for a plasma behaviour. If they could be significant, it is a result from a collective effect by the near-mode components, the relative phase among which is not randomized.

A control of the current density on the ribbon can be used for a wider range of modification. It is significant to change the ribbon width along with θ. On the contrary, in a usual design with a constant current density on the coil, the width $\Delta\varphi$ in the toroidal coordinates is modulated. It is known that the good quasi-symmetry is obtained by a control of the effective width using a split coil[6]; this is due to a partial return to the natural winding.

V. X-point and Helical divertor

A study of divertor action in a built-in divertor is one of the main experimental issues of the LHD project[3]. The magnetic configuration of LHD has been investigated to realize a divertor action as well as a stable high-beta plasma with good confinement and efficient heating[13]. The divertor in a helical device has been studied in relation to a scrape-off layer composed of the specific magnetic field with a long connection length to the wall. A Poincaré map of such field lines forms a peculiar area, such as a fish tail in Heliotron E, and it has been experimentally clarified that the plasma particles diffusing out of the main plasma flow along the area[15]. The analysis of the area with a long connection length is a very practical method for a design of a divertor[3,13].

The problem in this method would be that the connection length is not necessarily proportional to the flow along the field line. It will be true that there is an intense plasma-flow along a field line approaching the outer-most magnetic surface asymptotically. Further, the connection length in the neighborhood of the field is long and there will be a dense plasma similar to the edge plasma. However, the connection length of another field line approaching to another structure such as a magnetic island asymptotically might be comparable. On the other hand, the flow along a field line with an extremely-long connection length is not absurdly intense. Most of the particles diffusing into such an area will diffuse out of it after all rather than flow along the long field line. Hence, a field line which is sufficiently mixed up with that area and has only a short connection length is most important as a channel of the flow, if such a line exists.

The spectral definition of a magnetic field is not convenient for a general study of a divertor, because the divertor trace is conducted to an outer room where the spectral analysis is invalid. Also, the X-point itself, or the fixed point of order two in a Poincaré map, is sometimes located out of the convergence radius. Then, strictly speaking, it is impossible to describe X-point by the spectral components. However, if the high-j or high-n components are small enough, the description by truncated series is very useful, because magnetic field described by them is still a good model. On the other hand, since the X-point is located at a region with strong shear, an extremely accurate calculation enough to express the shear flow under a flux conserving condition is indispensable for a significant description of the X-point. The spectral model with a truncated series provides the accuracy.

A configuration model was introduced. It is artificially determined but is still similar to LHD. The major radius R_C is normalized to unity, and $\gamma_C \approx 1.25$ with $M=10/l=2$ is used. The helical coil is assumed to be wound with the natural winding law and to have a finite width defined by $\Delta\varphi=\pi/2M$ and a finite thickness determined by $0.20<\rho<0.30$. Then, only the spectral components with $n/j=2$ are still dominant. The poloidal field was assumed to be completely cancelled by external coils. Although the exact integration by Eq.(20) with respect to the coil width is possible, a numerical integration with respect to the coil thickness is necessary. The numerical integration was not treated seriously, because this is no more than a particular model. Also, only the spectral components with $|n|\leq 6$ and $j\leq 3$ were taken into account in the model, because all components with $j=4$ diminish in this model and the higher components which are variable according to a minor modification of the coil shape are not critical.

The magnetic surface of this model is shown in Fig.8. Owing to the symmetry, it is obvious that the theoretical X-point on the $w=\pi/M$ plane is on the $z=0$ line. It was found that the rotation of a field line in (ρ,u)-plane is very sensitive to the radius of the starting point. The exact X-point is determined by the rotation of $\Delta u=-\pi$ during a trace of one pitch ($\Delta w=2\pi/M$) starting from $w=\pi/M$. From a numerical trace of field lines near the X-point it was found that a cumulative error during the integration in one period is of the order of 10^{-9} or more and that the distance between too neighbouring points in a peculiar direction is expanded by 10^{6} times. A direct investigation of an X-point, or the fixed point of order two, is impossible even in the present model, because the random error in the first mapping will be expanded up to 10^{-3} after the second mapping; the result is almost meaningless. Figure 9 shows the trace of an X-point on the (ρ,u)-plane, where $X=\rho\cos u$ and $Y=\rho\sin u$ are used. The trace cannot be extended to the subsequent pitch, though the error could not be seen in the figure when that being drawn. An artificial elimination of the random error after the mapping was necessary to obtain a complete figure of the X-point.

First, an original figure (O) neighborhood of the outer X-point is mapped onto an extremely elongated ellipse (I) after one period. The two main axes AC and BD are indicated in the original figure. The axes are not symmetric with each other with respect to the inversion of the Y axis. This means that the axis does not coincide with the separatrix line; it is quite different from a conventional separatrix in a symmetric system. A mapping of the neighborhood of the X-point is well described by a linear mapping using a matrix expression. Similarly the mapping from the inner X-point to the outside is represented by a matrix.

Next, the product of the matrices gives the mapping around the fixed point of order two. The two main axes in the combined mapping are now symmetric and are the separatrix lines. A field line on the separatrix asymptotically approaches to the X-point, when w goes to either infinity or minus infinity. The field line departs from or approaches to the X-point most rapidly in the average during a couple of periods. However, it does not hold in a shorter interval. According with the precession of the local main axis a field line on the separatrix behaves as if it is outside or inside of a conventional separatrix. The resultant trace of a field line is complicated.

Finally, the mapping of the neighborhood of the X-point is examined by either a field trace or a matrix calculation depending on whether the displacement after the mapping is significant compared with the numerical error or not.

The notation T is used for a Poincaré map on the $w=\pi/M$ plane. Then, a fixed point of order two is defined by $TA_\infty = B_\infty$ and $TB_\infty=A_\infty$. If a point A_1

satisfies $\lim_{n\to\infty} T^{-2n}A_1=A_\infty$, it is on the separatrix in a conventional system. Since the separatrix is not closed in an asymmetric system, it is meaningless to distinguish the inside of it from the outside in a strict sense. However, the same term *separatrix* is used here. Figure 10 shows the *separatrix* on the $w=\pi/M$ plane. Since the separatrix has a intricate structure, it is significant as a conventional separatrix only when $T^{-2n}A_1$ is sufficiently close to an X-point for some primitive n and more. The separatrix line starting from the X-point rotates counter-clock-wise in the beginning. The left-hand side is the inside of the separatrix. Since the neighborhood of A_3 is mapped to a neighborhood of B_3, the outside region near A_3 is mapped to the inside of the separatrix. It forms a large crescent-shaped void just inside the outer X-point; the field line in the void is conducted to the outside of the separatrix during one period in the reversed direction. To find the forward image of the void, it is helpful to reverse the Y axis. The void in the reversed figure roughly overlaps with the original void. The overlapped region is a true void. Any field line in the true void has a short connection length from wall to wall. There are many voids with a higher order, i.e. the connection length is longer by the number of the order in pitches but insignificant for a plasma flow. Each of the voids has a considerable area, whereas the separating path between them has little measure, which causes the difficulty in the numerical pursuit of the exact position of the intricate *separatrix*. The top of the voids (near the points indicated by A's and B's) slides ever into the deep and may asymptotically touch the outer-most magnetic surface.

As known from a topological analysis[16,17], every order of *separatrix* passes from the outside to the inside and from the inside to the outside through a narrow channel between the separatrix and the outer edge of the primary void at B_3 (too narrow to be distinguished in the figure). The scrape-off layer with a considerable connection length is very narrow near the outer X-point in the present magnetic configuration. Moreover, it holds for each channel between the neighbouring voids. Those narrow channels include a field line with any range of connection length, though a statistical weight of each of those lines are negligibly small as already noted. Thus, the scrape-off layer between the conventional separatrix and the outer-most magnetic surface has a reticular structure.

On the other hand, the inner X-point in this figure has a rather wide stripe of scrape-off layer flowing out of the separatrix. It has an intricate and laminate structure. Moreover, a considerable gap connecting to the primary void is expected in the stripe. Although exact shape will be different in a different magnetic configuration, this structure of the helical divertor is unchanged.

As will be seen in Fig.9, the trace of the X-point is nearly on a constant-ρ surface. Thus, the deviation in ρ can be described as a perturbation. If the condition $Mw+2u=\pm\pi$ is satisfied at a point on the trace, B_ρ in Eq.(9) is zero for the dominant $n=2j$ terms, or $d\rho/dw=0$. Similarly, du/dw is almost constant. Hence, the condition $du/dw=-M/2$ determines the unperturbed X-point on a constant-ρ surface and keeping the relation $Mw+2u=\pm\pi$. The radius of the unperturbed X-point ρ_x is implicitly solved by

$$\left(\frac{\rho_x}{c}\right)^2=\left(\frac{2}{M}\right)^2\frac{Mh_1}{b-Mh_1}, \tag{21}$$

where $h_1=-\sum_j(-1)^j ja_{j,2j}\mathcal{Q}(\rho_x)$ is the relative strength of the helical field and the present value is evaluated from ρ_x as $Mh_1/b=0.59$. The primitive perturbation comes from a toroidal effect. The effect of the toroidal asymmetry in the resonant field ($n=2j$ components) is evaluated by leading terms in ρ/c.

$$\frac{1}{\rho_x}\frac{d\delta\rho}{dw}=-\mu\delta u \tag{22}$$

$$\frac{d\delta u}{dw}=-\nu\frac{\delta\rho}{\rho_x}+\varepsilon\cos\left(\frac{Mw}{2}-\frac{\pi}{2}\right), \tag{23}$$

where $\delta\rho$ and δu are the small deviation as a function of w, and the coefficients are given by $\mu=Mh_2/h_1$,

$$\nu=M\left[\frac{h_2}{h_1}\left(1+\frac{M^2\rho_x^2}{4c^2}\right)-1\right],\quad \varepsilon=\left(1+\frac{M^2\rho_x^2}{4c^2}\right)\frac{M\rho_x}{4c},\ \text{and}\ h_2=-\sum_j(-1)^j j^2 a_{j,2j}\mathcal{Q}(\rho_x).$$

This linear equation is easily solved as

$$\frac{\delta\rho}{\rho_x}=\frac{\varepsilon\mu}{\lambda^2+M^2/4}\cos\left(\frac{Mw}{2}-\frac{\pi}{2}\right)+C_1\exp\lambda w+C_2\exp-\lambda w, \tag{24}$$

$$\delta u=\frac{\varepsilon M/2}{\lambda^2+(M/2)^2}\sin\left(\frac{Mw}{2}-\frac{\pi}{2}\right)-\frac{\lambda}{\mu}C_1\exp\lambda w+\frac{\lambda}{\mu}C_2\exp-\lambda w, \tag{25}$$

where $\lambda=(\mu\nu)^{1/2}$, and C_1 and C_2 are arbitrary constants. Of course, the X-point is given by setting $C_1=0$ and $C_2=0$. Since the value of λ is about 20, the relative deviation due to the toroidal effect with the aspect ratio of about 5 is evaluated to be about one percent. The numerical result in Fig.9 is less than the evaluation. It is due to the off-resonant components. If they can be dealt with as a perturbation, the deviation is described by a similar equation with leading terms in ρ/c retained as

$$\frac{1}{\rho_x}\frac{d\delta\rho}{dw}=-\mu\delta u-\frac{Mh_n}{4h_1}\sin\,(pw+\frac{n\pi}{2}),\tag{26}$$

$$\frac{d\delta u}{dw}=-\nu\frac{\delta\rho}{\rho_x}+\frac{Mh_n}{4h_1}(1+\frac{2j}{n}\ \frac{M^2\rho_x^2}{4c^2})\cos\,(pw+\frac{n\pi}{2}).\tag{27}$$

where $p=(2j-n)M/2$, and h_n is the helical field with mode numbers j and n. Here, the X-point starting from the outside at $w=\pi/M$ is described. The solution is

$$\frac{\delta\rho}{\rho_x}=-\frac{Mh_n}{4h_1(\lambda^2+p^2)}[\mu(1-\frac{2j}{n}\frac{M^2\rho_x^2}{4c^2})+p]\cos\,(pw+\frac{n\pi}{2})\ +C_1\exp\lambda w\ +C_2\exp-\lambda w\tag{28}$$

$$\delta u=\frac{Mh_n}{4h_1(\lambda^2+p^2)}[-\nu+(1+\frac{2j}{n}\frac{M^2\rho_x^2}{4c^2})p]\sin\,(pw+\frac{n\pi}{2})\ -\frac{\lambda}{\mu}C_1\exp\lambda w\ +\frac{\lambda}{\mu}C_2\exp-\lambda w.\tag{29}$$

A fast oscillating perturbation is usually less effective to cause a deviation from the unperturbed line. It holds also in this case. However, it is a case with sufficiently off-resonant mode with $2j-n>4$, when the value of λ is about 20.

The location of the X-point is interesting for a design of baffles for a closed divertor. If the vacuum field is fixed, it is not difficult to adjust the location of the throat in the baffles. The great interest is in case of a scan of the vertical field, because it is an important method for a plasma control in an actual experiment. The vertical field dominantly changes the component $n=1/j=0$. Thus, the maximum shift of the X-point is evaluated from Eqs.(28) and (29) as $\delta\rho/R_c\approx\rho_x\delta u/R_c\approx0.002$ for the change $\Delta B_V/B_0\approx Mh_n/b=0.04$. This shows that the shift in a vertical field scan of 4% will be sufficiently small compared with the throat of 6cm gap vs. R_c=3.9m designed for LHD. A similar evaluation shows that the additive field from the induced current is not critical. Even if it includes a change in a resonant component, the solution is obtained from Eqs.(28) and (29) by setting $p=0$. The shift of the X-point is in the same level with slightly off-resonant components. For example, the shift is estimated to be $\delta\rho/R_c\approx0.002$, when a plasma current of 200kA happens to be induced in LHD.

The change due to a pitch modulation was demonstrated by an arbitrary change of helical components. The dominant change in the spectral composition is on $a_{1,1}$ and $a_{1,3}$, when a pitch modulation of the type $f(\theta)=\sin u$ is assumed. A small $n-1/j=1$ component in the natural winding was over-compensated (like in the case of $\alpha^*=0.1$) and $a_{1,3}$ was also adjusted accordingly with reference to Fig.4b. The resultant magnetic configuration is shown in Fig.11. The outer-most magnetic surface and the separatrix are significantly deformed owing to the change of the $n=3$ component. Of course, the basic structure of the separatrix remains unchanged. The divertor flow at the inner X-point becomes wider. The effect of the n=1 components on a shift of the X-point is hidden by a reverse shift due to the n=3 component. However, the effect is obvious in the core region, where the n=1 component overcomes the n=3 component owing to the different radial dependence. The shift of the magnetic axis from the origin, opposite to that in the original configuration, means a small helical excursion in the opposite phase.

VI. Summary and discussion

The classical representation of the vacuum magnetic field by the toroidal harmonic function is appropriate for a study of heliotron configuration. The present calculation of the function is satisfactory. The representation by the field component with both toroidal and poloidal mode numbers is a spectral analysis. The field generated by a helical winding with various winding laws can be analysed with sufficiently high accuracy. The toroidal coordinates is uniquely defined by a torus inscribed to the current-carrying coil. At the same time, the unique definition of the magnetic configuration is obtained. The natural winding defined by the simple winding law in the toroidal coordinates was found to provide a very pure set of the spectral components dominated by only the components resonant with the helicity of the helical coil. This provides a good quasi-symmetry, and is appropriate for a built-in divertor. A deviation from the natural winding causes a generation of a wide range of off-resonant components. The high accuracy of the model field was applied to a numerical study of a separatrix. The structure of a helical divertor was directly clarified by a numerical trace of the separatrix. The figure clearly shows the peculiar structure of the scrape-off layer in a helical divertor without symmetry. The complicated structure is unchanged by a perturbation field. A rigid baffle for a closed divertor is sufficiently usable even when various additional fields are expected in the operation.

The optimization study for LHD has been made within the criteria from the engineering accessibility of a superconducting helical coil. The flexibility in the design is greatly reduced, because the size of LHD is set near the lower limit for a superconducting coil system[13]. Although the parameter survey seems to have been rather point-wise, the machine parameters have been practically determined from a simple optimization analysis in the narrow accessible region. Since another design with a larger size permits much more flexibility in an engineering design, a flexible model of the magnetic configuration will be indispensable for a full survey for the optimization in future. The use of the toroidal harmonic functions is a promising choice for such a study.

The convergence of the series is essential in actual applications and more in the theoretical background of the analysis. Since a numerical calculation is inevitably an approximation, the truncation is one of the usual approximations. The accuracy greatly depends on the radial position to be investigated. It is satisfactorily good in the main plasma region with a small radius. Hence, the model will be better used in the equilibrium, stability and transport analyses of the plasma. On the contrary, the application to a helical divertor is rather restricted. It is not appropriate, for example, to determine the position of the divertor trace. However, the present description of a separatrix provides a different technique for the investigation of the helical divertor, instead of a field mapping which is a very time-consuming process. Moreover, it seems much helpful for the understanding of the structure.

Acknowledgments

The author wishes to thank Drs. J. Todoroki, Y. Nakamura, N. Ohyabu and K. Itoh for useful discussions. The computer system at NIFS Computer Center was used for the numerical calculation.

Appendix: Calculation of torus function

The derivative of a torus function (Legendre function with a half-integer order) can be expressed by the torus functions;

$$\frac{\partial Q^m_{n-1/2}(\cosh v)}{\partial v} = (n-m+\frac{1}{2}) \operatorname{cosech} v \; Q^m_{n+1/2}(\cosh v)$$

$$-(n+\frac{1}{2}) \coth v \; Q^m_{n-1/2}(\cosh v). \qquad (A1)$$

The torus functions were numerically calculated from an integral expression for non-negative m and n[8]:

$$Q^{m}_{n-1/2}(\cosh v)=\frac{(-1)^{m}\Gamma(n+m+1/2)}{2^{n+1/2}\,\Gamma(n+1/2)}\sinh^{m}v\int_{-1}^{1}\frac{(1-t^{2})^{n-1/2}}{(\cosh v-t)^{m+n+1/2}}dt \qquad \text{(A2)}$$

$$=(-1)^{m}\frac{\Gamma(n+m+1/2)}{\Gamma(n+1/2)}\frac{1}{(2\cosh v)^{n+1/2}}q_{m,n}(\cosh v),$$

$$q_{m,n}(\cosh v)=\int_{-1}^{1}\frac{\cosh^{n+1/2}v\sinh^{m}v\ (1-t^{2})^{n-1/2}}{(\cosh v-t)^{m+n+1/2}}dt. \qquad \text{(A3)}$$

Since $q_{m,n}(\cosh v)$ is a slowly varying function of the arguments, it is useful for a numerical calculation in a wide range of the arguments. The double exponential formula [a change of variable by $t=\tanh(\pi/2\ \sinh\tau)$][18] was used for a precise calculation. The values were checked by a couple of relations:

$$(n-m+\frac{1}{2})Q^{m}_{n+1/2}(z)-2nzQ^{m}_{n-1/2}(z)+(n+m-\frac{1}{2})Q^{m}_{n-3/2}(z)=0, \qquad \text{(A4)}$$

$$Q^{m+2}_{n-1/2}(z)+2(m+1)\frac{z}{(z^{2}-1)^{1/2}}Q^{m+1}_{n-1/2}(z)-(n-m-1/2)(n+m+1/2)Q^{m}_{n-1/2}(z)=0. \qquad \text{(A5)}$$

The relative error in the present calculation is speculated to be less than 4×10^{-14} in the limited parameter space: $\cosh v>4$, $m<256$, and $n<32$.

References

[1] K.Uo, Plasma Phys. 13 (1971) 243

[2] Lyon,J.F., Carreras,B.A., Chipley,K.K., et al., Fusion Technol. 10 (1986) 179

[3] Iiyoshi,A., Fujiwara,M., Motojima,O., Ohyabu,N., Yamazaki,K., Fusion Technol. 17 (1990) 169

[4] Nishimura,K., Matsuoka,K., Fujiwara,K., et al., Fusion Technol. 17 (1990) 86

[5] Lyon,J.F., Carreras,B.A., Dominguez,N., et al., Fusion Technol. 17, (1990) 188

[6] Nishimura,K., Fujiwara,M., Symmetrized Magnetic Field Configuration of Low Aspect Ratio Helical System, Rep. IPPJ-869 (Institute of Plasma Phys., Nagoya, 1988)

[7] Morse,P.M., Feshbach,H., Methods of Theoretical Physics II, McGraw-Hill, New York (1953) 1301

[8] Moriguchi,S., Udagawa,K., Hitotsumatsu,S., Sûgaku-kôshiki III (Mathematical formulae III, in Japanese), Iwanami, Tokyo (1960) 139

[9] Yoshikawa,S., Analytic Representation of Three Dimensional Stellarator Field, Rep. PPPL-2038, Princeton Plasma Phys. Lab., Princeton (1983)

[10] Nagasaki,K., Itoh,K., Wakatani,M., Iiyoshi,A., J. Phys. Soc. Japan 57 (1988) 2000

[11] Dommaschk,W., Comput. Phys. Comm. 40 (1986) 203

[12] Beidler,C., Grieger,G., Herrnegger,F., et al., Fusion Technol. 17 (1990) 148

[13] Yamazaki,K., Ohyabu,N., Okamoto,M., et al., in Proc. 13th Int. Conf. on Plasma Physics and Controlled Nuclear Fusion Research, IAEA-CN-53/C-4-11, Washington (1990)

[14]Obiki,T., Sudo,S., Sano,F., et al., in Proc. 13th Int. Conf. on Plasma Physics and Controlled Nuclear Fusion Research, IAEA-CN-53/C-1-1, Washington (1990)

[15] Obiki,T., Mizuuchi,T., Zushi,H., et al., in Plasma Physics and Controlled Nuclear Fusion Research 1988 (Proc. 12th Int. Conf. Nice, 1988), vol. II, IAEA, Vienna (1989) 337

[16] Morosov,A.I., Solov'ev,L.S., in Reviews of Plasma Physics vol.2, Consultants Bureau, New York (1966) 68

[17] Jackson,E.A., in Nagoya Lectures in Plasma Physics and Controlled Fusion (Ichikawa,Y.H., Kamimura,T., Ed.), Tokai Univ. Press, Tokyo (1989) 120

[18] Mori,M., FORTRAN 77 sûchikeisan puroguramingu (FORTRAN 77 Programming for Numerical Calculations, in Japanese), Iwanami, Tokyo (1986) 168

Figure Captions

Fig.1 Helical winding on a torus and the coordinates. The coil is assumed to be symmetric with respect to the inversion against x-axis. For an accurate calculation the helical current, added by virtual ring currents, is divided into basic current loops, each of which has the same shape as a unit current loop Δ. The cancel of the ring current is easy.

Fig.2 Spectral components for a filament current (a) with a simple winding and (b) with a natural winding, evaluated on the toroidal surface for the winding($\rho = a_c$). The field components with $0 \leq j < 64$ and $|n| < 64$ are analysed by the fast-fourier-transform. The parameters $M=10$, $l=2$ and $a_c/R_c=0.25$ are assumed.

Fig.3 Contour map of the systematic error due to truncation of the series in the case of the simple winding. The values show the relative error in logarithm. Although the accuracy is more than ten order of magnitude in the central region, it deteriorates rapidly as the radius increases. The comparison near the coil (indicated by X) is not valid, because the precise calculation from the Biot-Savart's formula is not tried there.

Fig.4 Pattern of spectral change due to pitch modulation. (a)Natural winding is used as an unmodulated standard because of the simple distribution. The change of each spectral components due to an infinitesimal modulation of the type: (b)$f(\theta)=\sin u$ and (c)$f(\theta)=\sin 2u$ is normalized by the amplitude α.

Fig.5 Spectral components of the standard configuration with the natural winding but in a frame with an improper axis c. When slightly larger c is used, the sharp ridge becomes greatly diffused. Since minimum radius ρ to the coil is now smaller than a_c, the convergence radius is smaller than a_c.

Fig.6 Effect of γ_c on dominant spectral components. This is valid for a particular case with $M=10/l=2$ and the natural winding.

Fig.7 Trajectory of the winding on (u,w)-plane for various winding laws: the natural winding(thick), the simple winding without(thin) and with the pitch modulation $\alpha^*=0.1$(dashed), $\alpha^*=0.2$(broken), and $\alpha^*=-0.1$(dot-dashed). Those are valid for a particular case with $M=10/l=2$ and $a_c/R_c=1/4$.

Fig.8 Magnetic surfaces and X-points (X) in the model field. The outer-most plot is almost the outer-most magnetic surface.

Fig.9 Projection of the X-point to the (ρ,u)-plane and the mapping from the neighborhood of the outer X-point(O) to the inside one(I). The points indicated by A, B, C and D show the correspondence. The points roughly show the direction of the main axes of the almost linear transform of this mapping.

Fig.10 X-points and separatrix in a helical divertor displayed on $w=\pi/M$ surface. The outer and inner X-points are indicated by A_∞ and B_∞, respectively. Two traces starting from each X-point are distinguished by the solid line and the broken line. The sequence of the mapping of a point A_1 is displayed as $TA_1=B_1$, $TB_1=A_2$, $TA_2=B_2$, ... etc. A particular point A_1 is chosen such that it is a leading point of the sinking separatrix. So, the series of the points are located at the top of each crescent-shaped "outside". A quite incomplete dotted-line(OMS) shows the outer-most magnetic surface.

Fig.11 Gross plot of magnetic surfaces and separatrix after the modification on the $n=1/j=1$ and $n=3/j=1$ components.

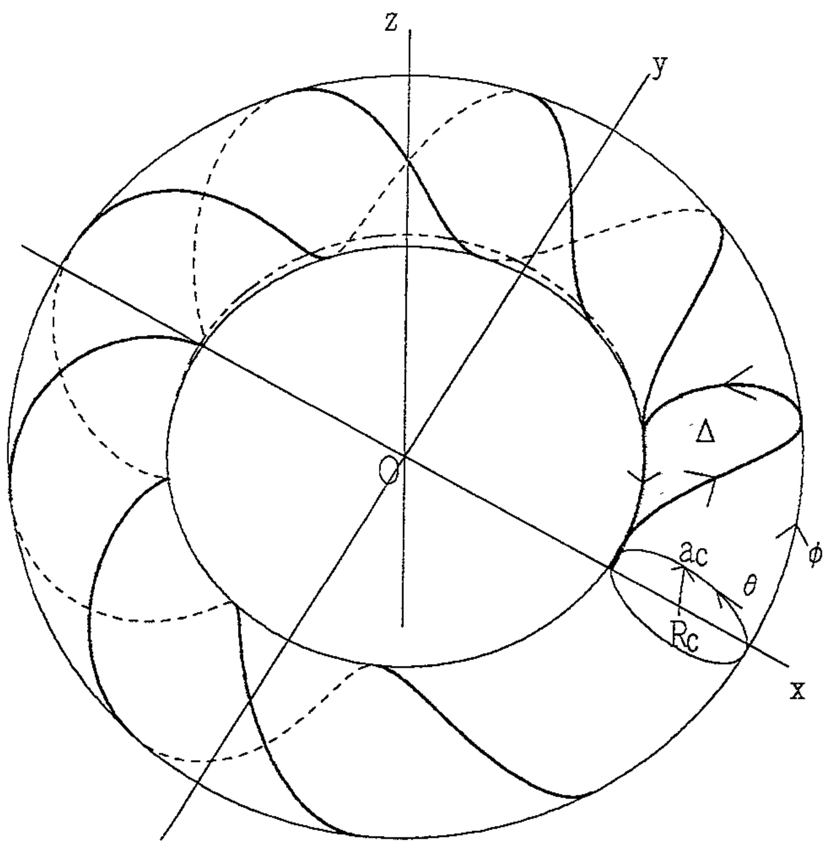

Fig.1

(a) simple

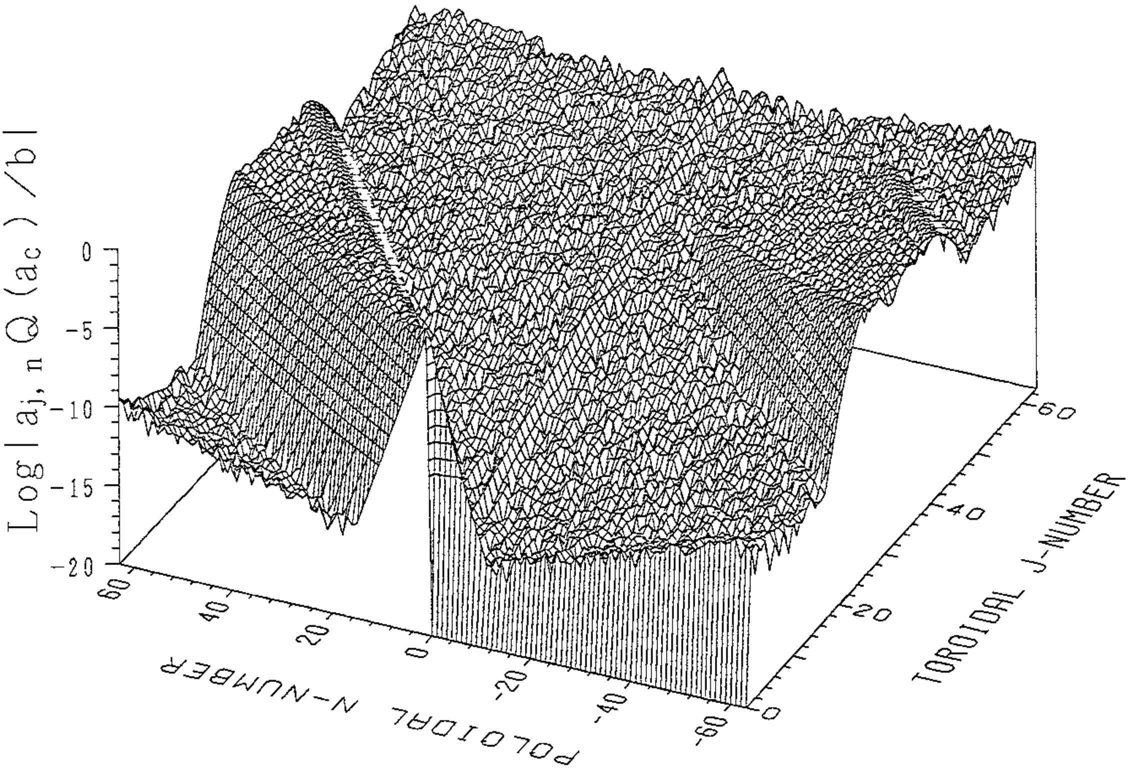

(b) natural

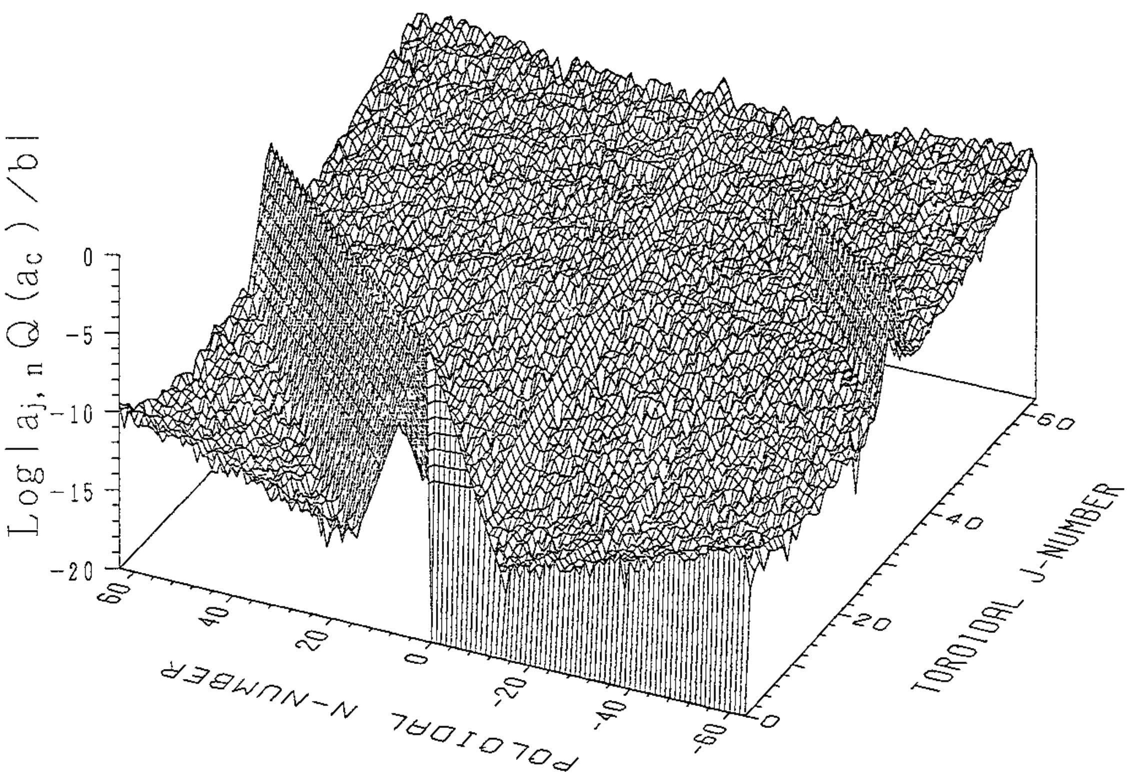

Fig.2

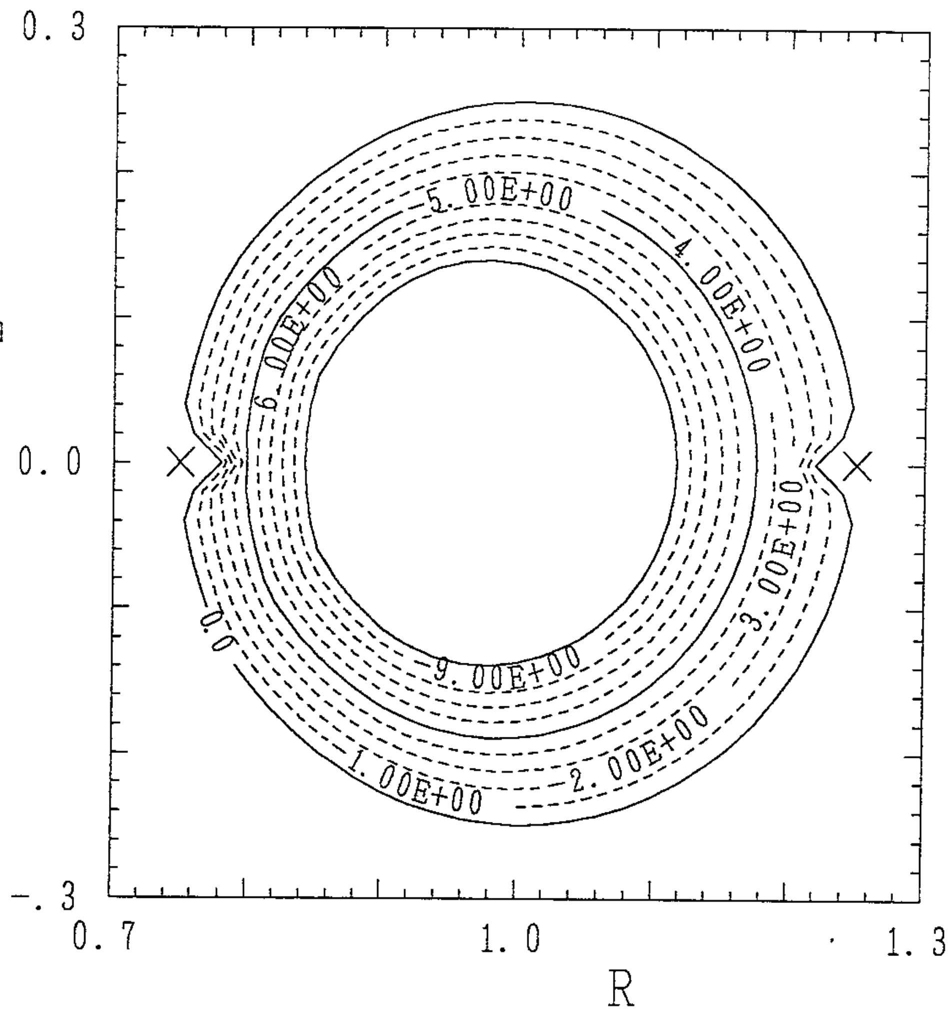
0. 3
0. 0
-. 3
Z
0. 7
1. 0
1. 3
R
5. 00E+00
4. 00E+00
6. 00E+00
3. 00E+00
0. 0
9. 00E+00
2. 00E+00
1. 00E+00

Fig.3

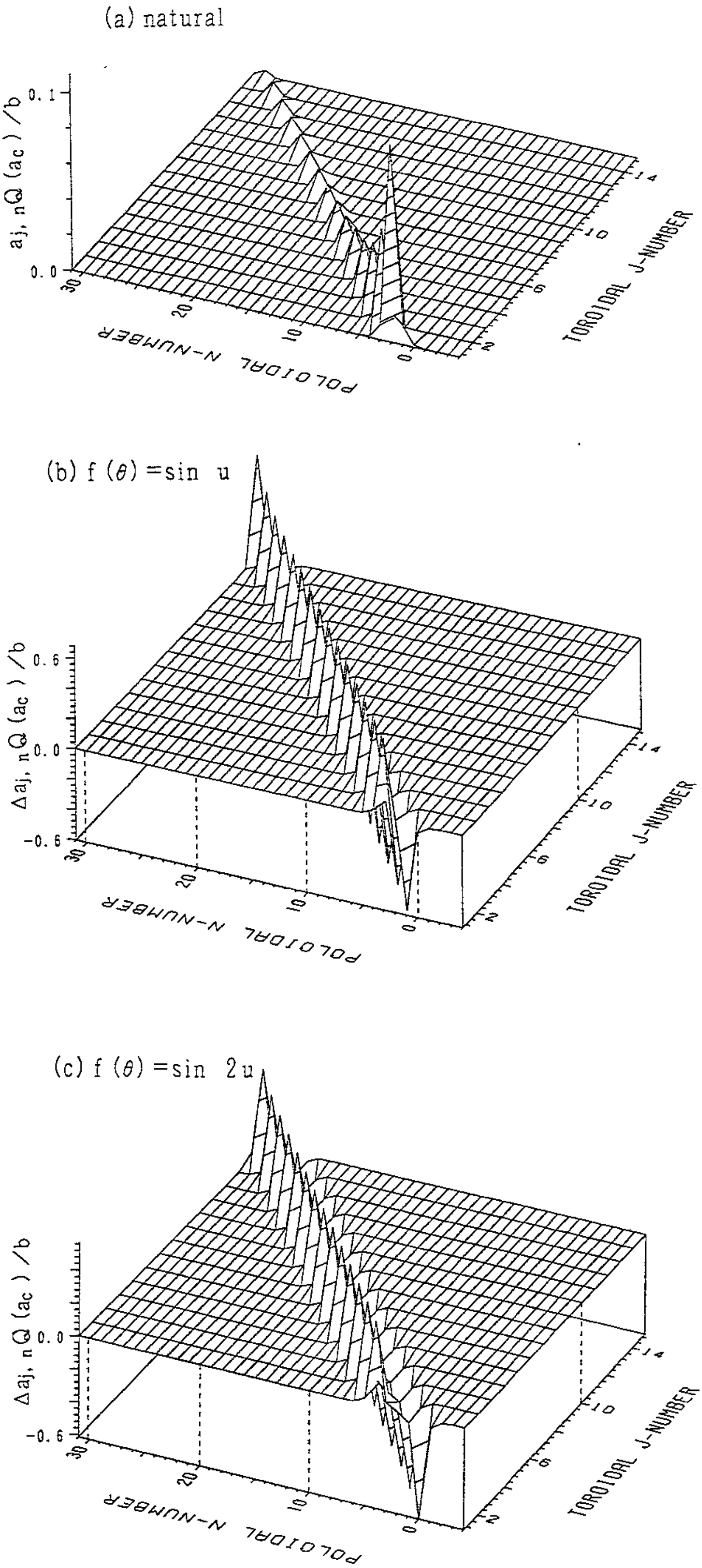
(a) natural
aj, nQ (ac) /b
0.1
0.0
30
20
10
0
POLOIDAL N-NUMBER
2
6
10
14
TOROIDAL J-NUMBER
(b) f (θ) =sin u
Δaj, nQ (ac) /b
0.6
0.0
-0.6
30
20
10
0
POLOIDAL N-NUMBER
2
6
10
14
TOROIDAL J-NUMBER
(c) f (θ) =sin 2u
Δaj, nQ (ac) /b
0.0
-0.6
30
20
10
0
POLOIDAL N-NUMBER
2
6
10
14
TOROIDAL J-NUMBER

Fig.4

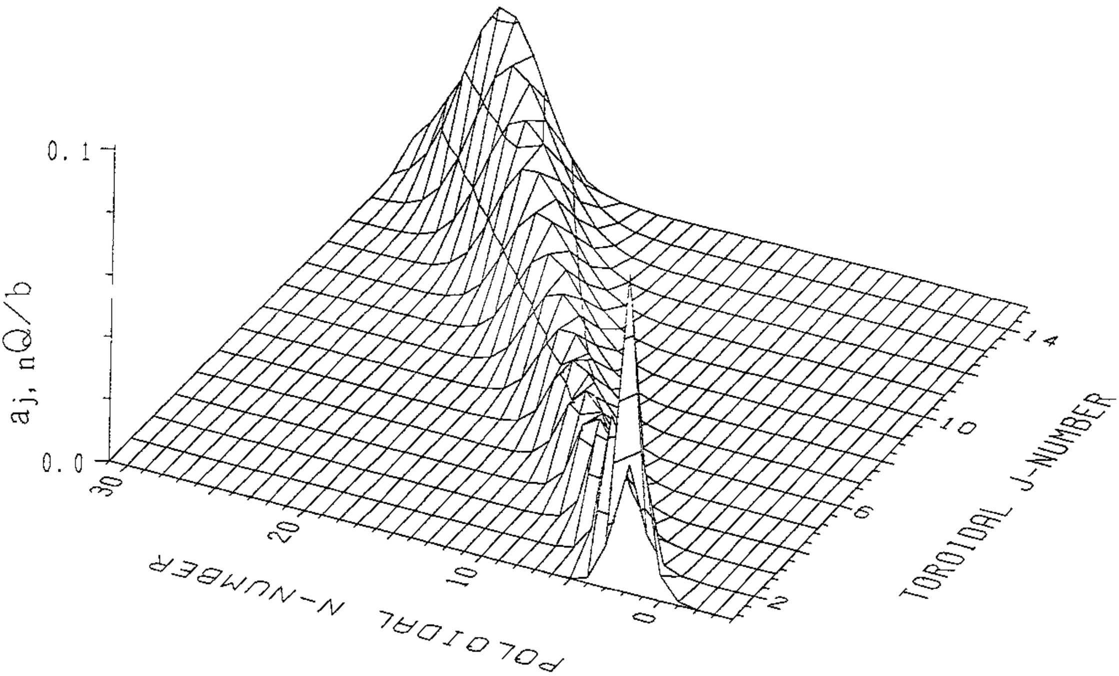
0.1
0.0
$a_{j,\,n}Q/b$
30
20
10
0
POLOIDAL N-NUMBER
2
6
10
14
TOROIDAL J-NUMBER

Fig.5

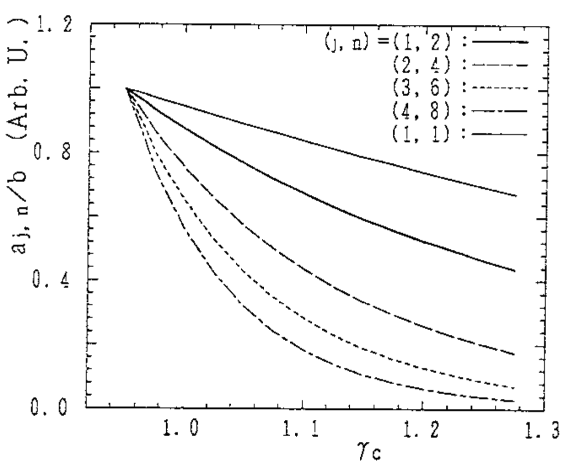
1.2
0.8
0.4
0.0
$a_{j,\,n}/b$ (Arb. U.)
1.0
1.1
1.2
1.3
γ_c
(j, n) = (1, 2) :
(2, 4) :
(3, 6) :
(4, 8) :
(1, 1) :

Fig.6

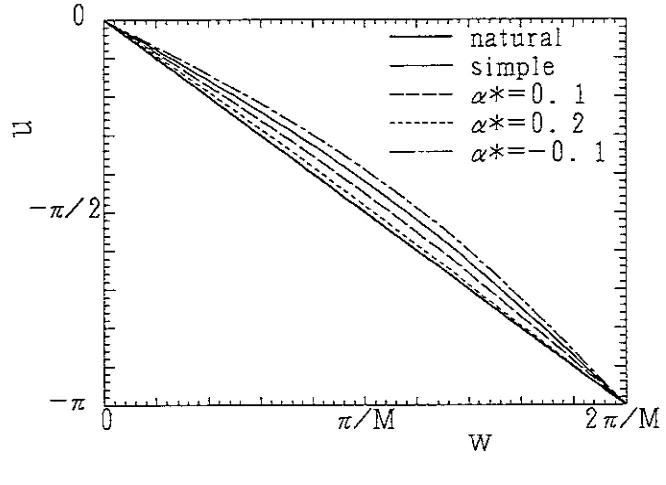

Fig.7

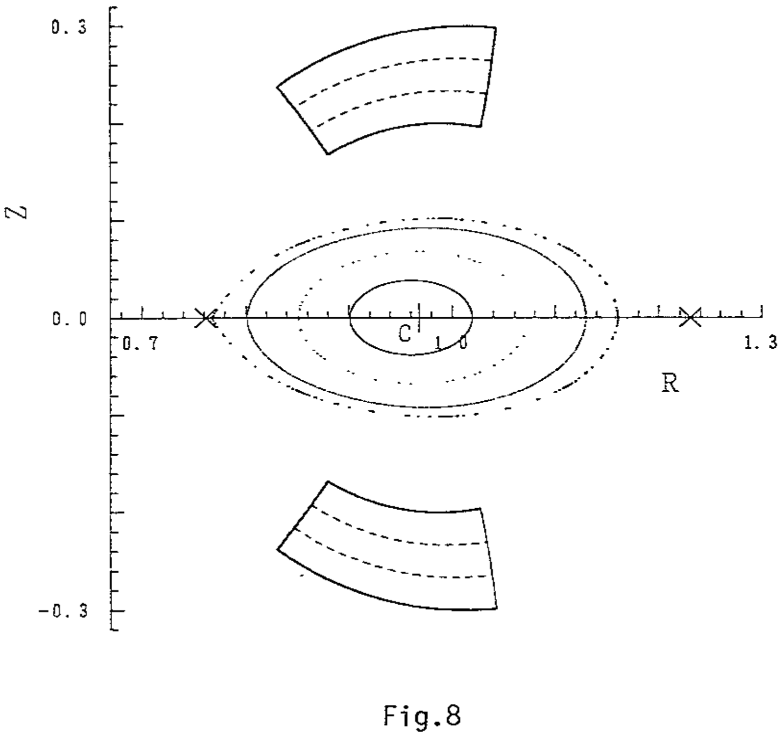

Fig.8

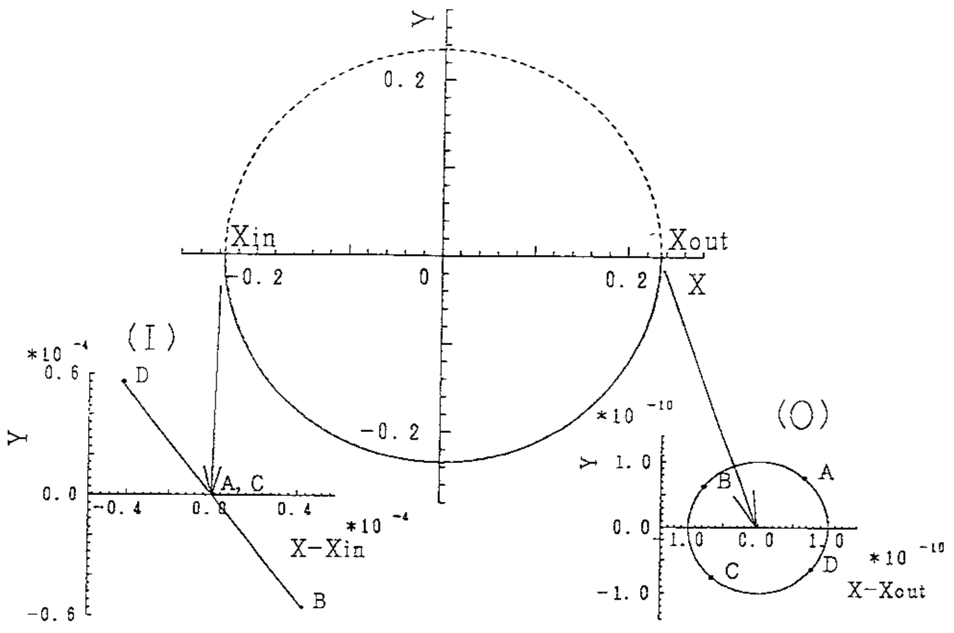

Y
0.2
Xin
Xout
-0.2
0
0.2
X
-0.2
(I)
*10 -4
0.6
D
Y
0.0
-0.4
0.0
0.4
A, C
*10 -4
X-Xin
-0.6
B
*10 -10
(O)
Y
1.0
B
A
0.0
-1.0
0.0
1.0
C
D
*10 -10
X-Xout
-1.0

Fig.9

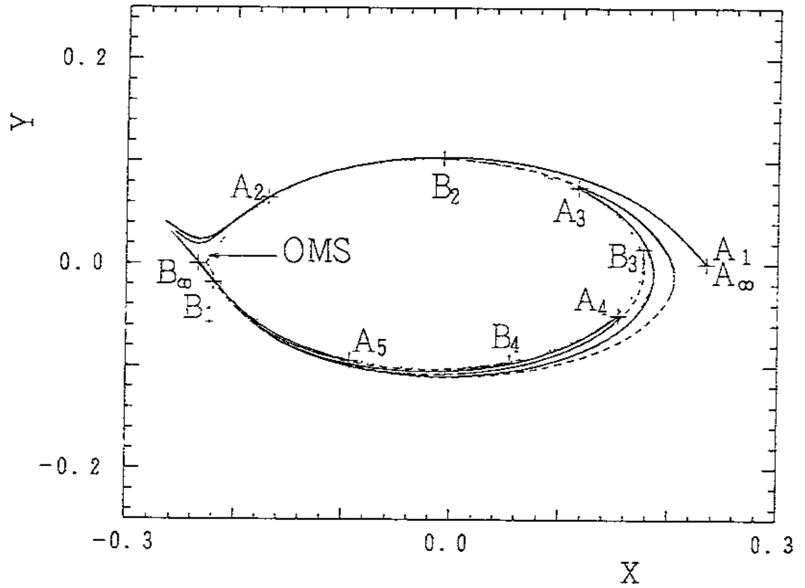

0.2
Y
0.0
-0.2
-0.3
0.0
0.3
X
A_2
B_2
A_3
B_3
A_1
A_∞
A_4
A_5
B_4
OMS
B_∞
B_1

Fig.10

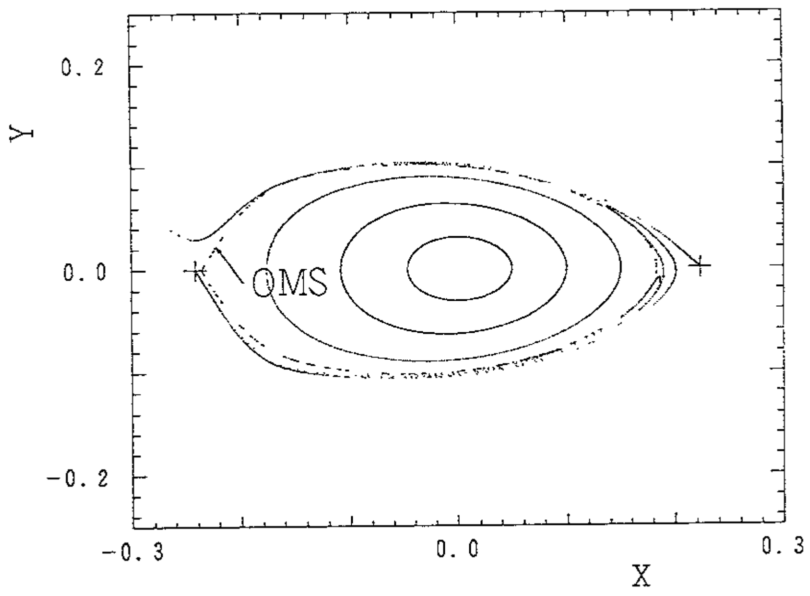

Fig.11

Recent Issues of NIFS Series

NIFS-25 B. Bhattacharya, T. Watanabe and Kyoji Nishikawa, *Single Particle and Fluid Picture for Ponderomotive Drift in Nonuniform Plasmas*; Apr. 1990

NIFS-26 K. Ida, S. Hidekuma, Y. Miura, T. Fujita, M. Mori, K. Hoshino, N. Suzuki, T. Yamaguchi and JFT-2M Group, *Edge Electron Field Profiles of H-mode Plasmas in JFT-2M Tokamak* ; Apr. 1990

NIFS-27 N. Nakajima and M. Okamoto, *Beam-Driven Currents in the 1/ ν Regime in a Helical System* ; Apr. 1990

NIFS-28 K. Itoh, K. Nagasaki and S.I. Itoh, *Heat Deposition on the Partial Limiter* ; Apr. 1990

NIFS-29 S.-I. Itoh A. Fukuyama adn K. Itoh, *Fokker-Plank Equation in the Presence of Anomallous Diffusion* ; May. 1990

NIFS-30 K. Yamazaki, O. Motojima, M. Asao, M. Fujiwara and A. Iiyoshi, *Design Scalings and Optimizations for Super-Conducting Large Helical Devices* ; May 1990

NIFS-31 H. Sanuki, T. Kamimura, K. Hanatani, K. Itoh and J. Todoroki, *Effects of Electric Field on Particle Drift Orbits in a l =2 Torsatron* ; May 1990

NIFS-32 Yoshi H. Ichikawa, *Experiments and Applications of Soliton Physics*; June 1990

NIFS-33 S.-I. Itoh, *Anomalous Viscosity due to Drift Wave Turbulence* ; June 1990

NIFS-34 K. Hamamatsu, A. Fukuyama, S.-I. Itoh, K. Itoh and M. Azumi, *RF Helicity Injection and Current Drive* ; July 1990

NIFS-35 M. Sasao, H. Yamaoka, M. Wada and J. Fujita, *Direct Extraction of a Na- Beam from a Sodium Plasma* ; July 1990

NIFS-36 N. Ueda, S.-I. Itoh, M. Tanaka and K. Itoh, *A Design Method of Divertor in Tokamak Reactors* Aug. 1990

NIFS-37 J. Todoroki, *Theory of Longitudinal Adiabatic Invariant in the Helical Torus*; Aug. 1990

NIFS-38 S.-I. Itoh and K. Itoh, *Modelling of Improved Confinements – Peaked Profile Modes and H-Mode–* ; Sep. 1990

NIFS-39 O. Kaneko, S. Kubo, K. Nishimura, T. Syoji, M. Hosokawa, K. Ida, H. Idei, H. Iguchi, K. Matsuoka, S. Morita, N. Noda, S. Okamura, T. Ozaki, A. Sagara, H. Sanuki, C. Takahashi, Y. Takeiri, Y. Takita, K. Tsuzuki, H. Yamada, T. Amano, A. Ando, M. Fujiwara, K. Hanatani, A. Karita, T. Kohmoto, A. Komori, K. Masai, T. Morisaki, O. Motojima, N. Nakajima, Y. Oka, M. Okamoto, S. Sobhanian and J. Todoroki, *Confinement Characteristics of High Power Heated Plasma in CHS*; Sep. 1990

NIFS-40 K. Toi, Y. Hamada, K. Kawahata, T. Watari, A. Ando, K. Ida, S. Morita, R. Kumazawa, Y. Oka, K. Masai, M. Sakamoto, K. Adati, R. Akiyama, S. Hidekuma, S. Hirokura, O. Kaneko, A. Karita, T. Kawamoto, Y. Kawasumi, M. Kojima, T. Kuroda, K. Narihara, Y. Ogawa, K. Ohkubo, S. Okajima, T. Ozaki, M. Sasao, K. Sato, K.N. Sato, T. Seki, F. Shimpo, H. Takahashi, S. Tanahashi, Y. Taniguchi and T. Tsuzuki, *Study of Limiter H- and IOC- Modes by Control of Edge Magnetic Shear and Gas Puffing in the JIPP T-IIU Tokamak*; Sep. 1990

NIFS-41 K. Ida, K. Itoh, S.-I. Itoh, S. Hidekuma and JIPP T-IIU & CHS Group, *Comparison of Toroidal/Poloidal Rotation in CHS Heliotron/Torsatron and JIPP T-IIU Tokamak*; Sep .1990

NIFS-42 T.Watari, R.Kumazawa,T.Seki, A.Ando,Y.Oka, O.Kaneko, K.Adati, R.Ando, T.Aoki, R.Akiyama, Y.Hamada, S.Hidekuma, S.Hirokura, E.Kako, A.Karita, K.Kawahata, T.Kawamoto, Y.Kawasumi, S.Kitagawa, Y.Kitoh, M.Kojima, T. Kuroda, K.Masai, S.Morita, K.Narihara, Y.Ogawa, K.Ohkubo, S.Okajima, T.Ozaki, M.Sakamoto, M.Sasao, K.Sato, K.N.Sato, F.Shinbo, H.Takahashi, S.Tanahashi, Y.Taniguchi, K.Toi, T.Tsuzuki, Y.Takase, K.Yoshioka, S.Kinoshita, M.Abe, H.Fukumoto, K.Takeuchi, T.Okazaki and M.Ohtuka, *Application of Intermediate Frequency Range Fast Wave to JIPP T-IIU and HT-2 Plasma*; Sep. 1990

NIFS-43 K.Yamazaki, N.Ohyabu, M.Okamoto, T.Amano, J.Todoroki, Y.Ogawa, N.Nakajima, H.Akao, M.Asao, J.Fujita, Y.Hamada, T.Hayashi, T.Kamimura, H.Kaneko, T.Kuroda, S.Morimoto, N.Noda, T.Obiki, H.Sanuki, T.Sato, T.Satow, M.Wakatani, T.Watanabe, J.Yamamoto, O.Motojima, M.Fujiwara, A.Iiyoshi and LHD Design Group, *Physics Studies on Helical Confinement Configurations with l=2 Continuous Coil Systems*; Sep. 1990

NIFS-44 T.Hayashi, A.Takei, N.Ohyabu, T.Sato, M.Wakatani, H.Sugama, M.Yagi, K.Watanabe, B.G.Hong and W.Horton, *Equilibrium Beta Limit and Anomalous Transport Studies of Helical Systems*; Sep. 1990

NIFS-45 R.Horiuchi, T.Sato, and M.Tanaka, *Three-Dimensional Particle Simulation Study on Stabilization of the FRC Tilting Instability*; Sep. 1990

NIFS-46 K.Kusano, T.Tamano and T. Sato, *Simulation Study of Nonlinear Dynamics in Reversed-Field Pinch Configuration*; Sep. 1990

NIFS-47 Yoshi H.Ichikawa, *Solitons and Chaos in Plasma*; Sep. 1990

NIFS-48 T.Seki, R.Kumazawa, Y.Takase, A.Fukuyama, T.Watari, A.Ando, Y.Oka, O.Kaneko, K.Adati, R.Akiyama, R.Ando, T.Aoki, Y.Hamada, S.Hidekuma, S.Hirokura, K.Ida, K.Itoh, S.-I.Itoh, E.Kako, A. Karita, K.Kawahata, T.Kawamoto, Y.Kawasumi, S.Kitagawa, Y.Kitoh, M.Kojima, T.Kuroda, K.Masai, S.Morita, K.Narihara, Y.Ogawa, K.Ohkubo, S.Okajima, T.Ozaki, M.Sakamoto, M.Sasao, K.Sato, K.N.Sato, F.Shinbo, H.Takahashi, S.Tanahashi, Y.Taniguchi, K.Toi and T.Tsuzuki, *Application of Intermediate Frequency Range Fast Wave to JIPP T-IIU Plasma*; Sep.1990

NIFS-49 A.Kageyama, K.Watanabe and T.Sato, *Global Simulation of the Magnetosphere with a Long Tail: The Formation and Ejection of Plasmoids*; Sep.1990

NIFS-50 S.Koide, *3-Dimensional Simulation of Dynamo Effect of Reversed Field Pinch*; Sep. 1990

NIFS-51 O.Motojima, K. Akaishi, M.Asao, K.Fujii, J.Fujita, T.Hino, Y.Hamada, H.Kaneko, S.Kitagawa, Y.Kubota, T.Kuroda, T.Mito, S.Morimoto, N.Noda, Y.Ogawa, I.Ohtake, N.Ohyabu, A.Sagara, T. Satow, K.Takahata, M.Takeo, S.Tanahashi, T.Tsuzuki, S.Yamada, J.Yamamoto, K.Yamazaki, N.Yanagi, H.Yonezu, M.Fujiwara, A.Iiyoshi and LHD Design Group, *Engineering Design Study of Superconducting Large Helical Device*; Sep. 1990

NIFS-52 T.Sato, R.Horiuchi, K. Watanabe, T. Hayashi and K.Kusano, *Self-Organizing Magnetohydrodynamic Plasma*; Sep. 1990

NIFS-53 M.Okamoto and N.Nakajima, *Bootstrap Currents in Stellarators and Tokamaks*; Sep. 1990

NIFS-54 K.Itoh and S.-I.Itoh, *Peaked-Density Profile Mode and Improved Confinement in Helical Systems*; Oct. 1990

NIFS-55 Y.Ueda, T.Enomoto and H.B.Stewart, *Chaotic Transients and Fractal Structures Governing Coupled Swing Dynamics*; Oct. 1990

NIFS-56 H.B.Stewart and Y.Ueda, *Catastrophes with Indeterminate Outcome*; Oct. 1990

NIFS-57 S.-I.Itoh, H.Maeda and Y.Miura, *Improved Modes and the Evaluation of Confinement Improvement*; Oct. 1990

NIFS-58 H.Maeda and S.-I.Itoh, *The Significance of Medium- or Small-size Devices in Fusion Research*; Oct. 1990

NIFS-59 A.Fukuyama, S.-I.Itoh, K.Itoh, K.Hamamatsu, V.S.Chan, S.C.Chiu, R.L.Miller and T.Ohkawa, *Nonresonant Current Drive by RF Helicity Injection*; Oct. 1990

NIFS-60 K.Ida, H.Yamada, H.Iguchi, S.Hidekuma, H.Sanuki, K.Yamazaki and CHS Group, *Electric Field Profile of CHS Heliotron/Torsatron Plasma with Tangential Neutral Beam Injection*; Oct. 1990

NIFS-61 T.Yabe and H.Hoshino, *Two- and Three-Dimensional Behavior of Rayleigh-Taylor and Kelvin-Helmholz Instabilities*; Oct. 1990

NIFS-62 H.B. Stewart, *Application of Fixed Point Theory to Chaotic Attractors of Forced Oscillators;* Nov. 1990

NIFS-63 K.Konn., M.Mituhashi, Yoshi H.Ichikawa,*Soliton on Thin Vortex Filament;* Dec. 1990

NIFS-64 K.Itoh, S.-I.Itoh and A.Fukuyama,*Impact of Improved Confinement on Fusion Research;* Dec. 1990

NIFS -65 A.Fukuyama, S.-I.Itoh and K. Itoh,*A Consistency Analysis on the Tokamak Reactor Plasmas;* Dec. 1990

NIFS-66 K.Itoh, H. Sanuki, S.-I. Itoh and K. Tani,*Effect of Radial Electric Field on α-Particle Loss in Tokamaks;* Dec. 1990

NIFS-67 K.Sato,and F.Miyawaki,*Effects of a Nonuniform Open Magnetic Field on the Plasma Presheath*; Jan.1991

NIFS-68 K.Itoh and S.-I.Itoh,*On Relation between Local Transport Coefficient and Global Confinement Scaling Law;* Jan. 1991

NIFS-69 T.Kato, K.Masai, T.Fujimoto,F.Koike, E.Källne, E.S.Marmar and J.E.Rice,*He-like Spectra Through Charge Exchange Processes in Tokamak Plasmas;* Jan.1991

NIFS-70 K. Ida, H. Yamada, H. Iguchi, K. Itoh and CHS Group, *Observation of Parallel Viscosity in the CHS Heliotron/Torsatron* ; Jan.1991